PHYSICS OF FLUIDS **18**, 103304 (2006)
(Received 27 January 2006; accepted 22 September 2006; published online 26 October 2006)

Dynamics of a two-dimensional upflowing mixing layer seeded with bubbles: Bubble dispersion and effect of two-way coupling

E. Climentᵃ⁾
Laboratoire de Génie Chimique UMR CNRS 5503, 5, rue Paulin Talabot, 31106 Toulouse, France

J. Magnaudetᵇ⁾
Institut de Mécanique des Fluides de Toulouse UMR CNRS 5502, Allée du Professeur Camille Soula, 31400 Toulouse, France

The evolution and structure of a spatially evolving two-dimensional mixing layer seeded with small bubbles are numerically investigated. The one-way coupling approach is first employed to show that characteristics of bubble dispersion are dominated by the possibility for sufficiently small bubbles to be captured in the core of the vortices. A stability analysis of the ordinary differential equation system governing bubble trajectories reveals that this entrapment process is governed by the presence of stable fixed points advected by the mean flow. Two-way coupling simulations are then carried out to study how the global features of a two-dimensional flow are affected by bubble-induced disturbances. The local interaction mechanism between the two phases is first analyzed using detailed simulations of a single bubbly vortex. The stability of the corresponding fixed point is found to be altered by the collective motion of bubbles. For trapped bubbles, the interphase momentum transfer yields periodic sequences of entrapment, local reduction of velocity gradients, and eventually escape of bubbles. Similar mechanisms are found to take place in the spatially evolving mixing layer. The presence of bubbles is also found to enhance the destabilization of the inlet velocity profile and to shorten the time required for the rollup phenomenon to occur. The most spectacular effects of small bubbles on the large-scale flow are a global tilting of the mixing layer centerline towards the low-velocity side and a strong increase of its spreading rate. In contrast, no significant modification of the flow is observed when the bubbles are not captured in the large-scale vortices, which occurs when the bubble characteristics are such that the drift parameter defined in the text exceeds a critical value. These two contrasted behaviors agree with available experimental results.

I. INTRODUCTION

Two-phase dispersed flows are of major importance in a wide variety of industrial and natural processes. For instance full-scale devices in chemical engineering plants have to be carefully designed to achieve optimal mixing, mass transfer, or chemical reaction. Transport and extraction of oil are always performed under two-phase flow conditions. In such systems, predicting the phase distribution and the macroscopic evolution of the bulk flow is still a challenging task. The presence of a dispersed phase made of particles, droplets, or bubbles, dramatically affects the global properties of the flow. Conversely, the dispersion of the particulate phase is mainly related to the dynamics of the carrying flow. A naive analysis would conclude that turbulence mixes the entire flow and yields a uniform distribution of the dispersed phase. However, detailed analysis contradicts this conclusion, as shown by Eaton and Fessler[1] for particulate flows or by Spelt and Biesheuvel[2] for bubbles (see also Davila and Hunt[3]). Turbulent structures induce preferential accumulation of particles in well-defined structures of the flow. Hence, the local value of bulk properties such as density, effective viscosity, or thermal diffusion depends on the local volume fraction of the particulate phase. Even at modest concentration, two-way coupling interactions may modify the dynamics of vortical structures of the carrying flow.[4] These interactions are very difficult to take into account in global models because of the large variety of length scales involved in the momentum transfer between the dispersed and the continuous phase. For instance, bubbles and particles induce small-scale velocity fluctuations in their vicinity. Part of the energy due to the wake and the boundary layer is locally and almost immediately dissipated. However, collective effects can feed the low-wavenumber contents of the energy spectrum through backscatter transfer, making the overall response of the flow difficult to predict.

Very few available experimental studies have provided simultaneous measurements of both phases.[4,5] This is mainly because the presence of particles or bubbles in the flow decreases the accuracy of most nonintrusive measuring techniques or even prevents their use. Based on particle image velocimetry (PIV) measurements and optical filtering, Ford and Loth[6] and Dreier *et al.*[7] extracted the fluid velocity field together with Lagrangian trajectories of the dispersed phase in a plane horizontal mixing layer. Using a phase Doppler particle analyzer (PDPA), Martinez-Bazan and Lasheras[8] and

ᵃ⁾Electronic mail: eric.climent@ensiacet.fr
ᵇ⁾Electronic mail: magnau@imft.fr

Rightley and Lasheras[5] determined bubble dispersion and interphase coupling in the same flow configuration. Bubble concentration profiles were found to satisfy self-similarity conditions. These measurements also revealed that bubbles are entrained by the large-scale vortices, which results in a nonuniform spatial distribution of the dispersed phase.

Numerical simulation of dispersed two-phase flows has also provided insightful results over the past two decades. Lagrangian tracking of small particles moving in a known velocity field was first performed[9–11] to demonstrate that segregation and dispersion properties of the particulate phase are basically related to the characteristics of the vortices. The major role played by vortical structures was widely emphasized in various carrying flows.[12–14] Inertial particles or massless bubbles experience dominant forces of a different nature. Heavy particles are swept outside vortices and accumulate in straining regions through centrifugal ejection. In contrast, bubbles tend to accumulate within the vortex cores because they are mainly driven by the added-mass force which is directed toward the high-vorticity regions. Both features have been widely observed experimentally, and Lagrangian tracking based on simple force balances reproduces qualitatively the underlying physics. With the considerable increase of computational resources, unsteady three-dimensional flows were then considered by solving directly the full Navier-Stokes equations. Using the concept of point forces to model the effect of small heavy particles on the flow field, modulation of turbulence properties in homogeneous situations[15,16] or in channel flows[17] was investigated. In bubbly flows, bubbles can drive the large-scale fluid motions through collective buoyancy effects and can simultaneously contribute to the small-scale agitation due to wake and path instabilities. As for turbulent particulate flows, the dynamics of turbulent bubbly flows is greatly complicated by the continuous range of spatial scales involved in the energy transfer process. Even though a Kolmogorov scaling has been clearly identified for the dispersion of small bubbles, bubble-induced modifications in a fully turbulent flow are still under examination.[18] Moreover, compared with the case of heavy solid particles, bubbles represent a much more difficult problem because they are extremely sensitive to hydrodynamic effects, owing to their negligible density. While part of these effects, i.e., added mass, is now quite well known, models for the lift force in a general flow field are still lacking in several flow regimes, especially for microbubbles. The study of relatively simple bubbly flows in a regime where the hydrodynamic forces are reasonably well known is thus of great interest to identify and quantify interaction mechanisms. A plane mixing layer can be regarded as a canonical case of free-shear flow where well-defined coherent structures drive the dispersion features and interphase coupling governs the evolution of large-scale vortices seeded with bubbles.

The computations reported below provide new insights to interpret available, apparently conflicting, experimental results.[19,20] The first attempt to perform two-way coupling simulations in a bubbly mixing layer was achieved by Ruetsch and Meiburg.[21] The idealized temporal mixing layer[22,23] is a useful configuration but it obviously prevents the investigation of the spatial evolution of large-scale dynamics. Druzhinin and Elgobashi[24] recently achieved a three-dimensional computation of a two-phase mixing layer. Their approach makes use of a mixed Lagrangian-Eulerian formulation which reproduces bubble accumulation in vortex cores without inducing numerical instabilities on the Eulerian concentration. Their results reveal that a nonuniform bubble concentration profile at the inflow strongly affects the velocity fluctuations throughout the flow and that the growth of the vorticity thickness of the mixing layer is driven by unstable bulk stratification.

In the present paper we report on a two-way coupling investigation of an upward spatially evolving two-dimensional mixing layer seeded with bubbles. All bubbles are assumed to have the same diameter; however, the role of the bubble diameter is investigated through different runs. This is why the present study is quite complementary from that in Ref. 24, where all the computations were run with the same bubble diameter. Based on the numerical results, we carry out a detailed analysis of bubble dispersion induced by the large-scale vortices and of bubble-induced modifications on both the vortical structure and the global characteristics of the large-scale flow.

II. INTERPHASE COUPLING APPROACH

A. Lagrangian tracking

The dispersed phase is made of small bubbles experiencing the combined effects of the carrying fluid flow and the buoyancy force. Bubble trajectories are distinct from fluid element paths and a precise force balance acting on the bubbles is required. Obtaining an analytical expression for all hydrodynamic forces is still an open issue in most flow regimes, even though problems linked with deformability, breakup, coalescence, collisions, and contamination by surfactants are disregarded. Therefore, assumptions have to be made to simplify the problem and obtain a reasonable force balance. Considering only bubbles smaller than all the relevant spatial length scales of the carrying flow makes the so-called Fàxen corrections induced by the local curvature of the flow velocity field negligible.[25,26] Moreover, restricting ourselves to situations where the bubble Reynolds number (defined below) is typically a few hundreds allows us to write the force balance as a sum of distinct contributions. This is due to two crucial factors. First, bubbles rising in low-viscosity liquids such as water are almost spherical in this range and do not exhibit path instability.[27] Second, the mechanisms that control lift effects in this range are essentially of inviscid nature, so that the inviscid expression of the lift force is appropriate.[28] Note that this is not the case for bubble Reynolds numbers typically less than unity, in which case viscosity and inertia play a joint role and combine in a nonlinear way in the generation of lift effects, making the inertial scaling or even the sign of the force predicted by the inviscid expression irrelevant.[29] Hence, assuming that bubbles keep a spherical shape, we can track their trajectories and predict the position $\mathbf{x}(t)$ of their center of mass and their velocity $\mathbf{v}(t)$ in a fluid flow whose velocity, Lagrangian

acceleration, and vorticity at $\mathbf{x}(t)$ are, respectively, $\mathbf{u}$, $D\mathbf{u}/Dt$, and $\boldsymbol{\omega}=\nabla\times\mathbf{u}$, by solving the differential system [Eqs. (1) and (2)] for each bubble,

$$\frac{d\mathbf{x}}{dt}=\mathbf{v},\quad \rho_p V\frac{d\mathbf{v}}{dt}=\mathbf{F}, \tag{1}$$

$$\mathbf{F}=(\rho_p-\rho_f)V\mathbf{g}+\rho_f\frac{D\mathbf{u}}{Dt}-\rho_f\frac{3V}{8R}C_D|\mathbf{v}-\mathbf{u}|(\mathbf{v}-\mathbf{u})$$
$$+\rho_f V C_M\left(\frac{D\mathbf{u}}{Dt}-\frac{d\mathbf{v}}{dt}\right)-\rho_f V C_L(\mathbf{v}-\mathbf{u})\times\boldsymbol{\omega}, \tag{2}$$

where ρ_p (respectively, ρ_f) denotes the bubble (respectively, liquid) density, and V and R are the bubble volume and radius, respectively. C_D, C_M, and C_L are the drag, added-mass, and lift coefficients, respectively. In addition to the restrictions discussed above, Eqs. (1) and (2) rely on several important assumptions. First, they assume that direct interactions between bubbles are negligible. Neglecting coalescence, breakup, collisions, and direct hydrodynamic interactions restricts our investigation to configurations with low bubble volume fractions. Then, the force balance (1) and (2) is based on the velocity and velocity gradients of the undisturbed flow field, which means that two-way coupling effects only modify the flow through collective effects, whereas the disturbance of the large-scale flow due to a single bubble is assumed to be negligibly small. The various forces taken into account in Eq. (2) are the buoyancy force, the so-called pressure gradient force due to the Lagrangian acceleration of fluid elements, the viscous drag force, the added-mass force, and the inertial lift force. In the above expression, the drag coefficient C_D depends on the instantaneous bubble Reynolds number $\mathrm{Re}_p=2|\mathbf{v}-\mathbf{u}|R/\nu$ (ν being the kinematic viscosity of the carrying fluid). Based on direct numerical simulations around a single bubble,[30] an accurate approximation of $C_D(\mathrm{Re}_p)$ is

$$C_D(\mathrm{Re}_p)=16(1+0.15\,\mathrm{Re}_p^{1/2})/\mathrm{Re}_p \quad \text{for } \mathrm{Re}_p<50, \tag{3a}$$

$$C_D(\mathrm{Re}_p)=48(1-2.21\,\mathrm{Re}_p^{-1/2})/\mathrm{Re}_p \quad \text{for } \mathrm{Re}_p>50. \tag{3b}$$

Note that Eq. (3b) is simply the theoretical result established by Moore[31] in the limit of very large Reynolds number, which was actually shown in Ref. 30 to be valid even at moderate Reynolds number. In the range of high bubble Reynolds numbers ($200<\mathrm{Re}_p<500$), the contribution of unsteady viscous effects to the total drag force is weak. Using direct numerical simulation around a single bubble in an oscillating flow, Rivero *et al.*[32] showed that the history force may be neglected for moderate accelerations of the bubble at such high Re_p. The added-mass coefficient C_M is now known to be constant and equal to $1/2$ whatever the Reynolds number.[28,32] In contrast, it was found in Ref. 33 that the lift coefficient C_L is a function of both the Reynolds number and the shear rate. However, both dependencies are weak for $\mathrm{Re}_p>10$, so that in the present context it is appropriate to consider C_L as a constant whose value corresponds to the inviscid lift coefficient in a weak shear flow, i.e., $C_L=1/2$ (Ref. 34). As mentioned above, the computations discussed below focus on moderate-to-high bubble Reynolds number. More precisely, Re_p ranges typically from 200 to 600, which in pure water corresponds to equivalent bubble diameters ranging from 500 μm to 1.5 mm, approximately. Bubble deformation is moderate in this range and is thus neglected as a first approximation. The 1.5-mm bubble case is obviously the most critical as deformation does occur in air-water flows. We neglect this aspect of the bubbly flow because we mostly aim at investigating the relationship between the bubble drift parameter and the two-way coupling modifications of the flow.

As $\rho_p\ll\rho_f$, Eqs. (1) and (2) may be simplified, yielding

$$\frac{d\mathbf{x}}{dt}=\mathbf{v},$$
$$C_M\frac{d\mathbf{v}}{dt}=-\mathbf{g}+(1+C_M)\frac{D\mathbf{u}}{Dt}-\frac{3}{8R}C_D|\mathbf{v}-\mathbf{u}|(\mathbf{v}-\mathbf{u}) \tag{4}$$
$$-C_L(\mathbf{v}-\mathbf{u})\times\boldsymbol{\omega}.$$

All forces in Eq. (4) are evaluated using the characteristics of the instantaneous flow field at the exact position $\mathbf{x}$ of the bubble. Since the bubble location generally differs from the location of the mesh grid points used in the flow simulation, an interpolation procedure is required. A bicubic spline interpolation involving 64 nodes is employed to ensure the accuracy and the stability of the trajectory computation. The set of ordinary differential equations (ODEs) (4) is solved using a fourth-order Runge-Kutta scheme. Parallelization is employed to compute simultaneously all bubble trajectories. In the two-way coupling computations of Sec. IV B, the number of bubbles is $O(10^5)$.

B. Large-scale Navier-Stokes equations and coupling terms

To solve (4), the instantaneous motion of the carrying phase is required. Assuming that the flow is incompressible and Newtonian, its motion can be predicted by solving the full unsteady Navier-Stokes equations. However, as mentioned in the introduction, the small-scale motions induced by the dispersed phase cannot in general be resolved, owing to limitations in computer resources. Therefore, it is necessary to filter the local equations of the flow field at a certain scale λ. Bubbles act on the flow through different mechanisms. Some of them are directly related to the actual size of the bubbles. Boundary layers, near-wake effects, and potential flow disturbances around a moving bubble all scale with the bubble radius R and are not directly considered here. On the other hand, collective effects that occur through smooth variations of the bubble concentration have a significant impact on the large-scale fluid motion (see, for example, bubble columns or fluidized bed instabilities). As we are only interested in such collective effects, λ is chosen such that $L\gg\lambda\gg R$, where L stands for the characteristic scale of the large-scale velocity gradients. This obviously imposes an upper bound on the grid cell size. Based on several preliminary tests, we found that the grid spacing has to be typically ten times larger than R. The filtered fluid velocity field $\langle\mathbf{u}\rangle$ (the

brackets denote the spatial filtering at scale λ) is obtained by solving the continuity equation (5a) and the fluid momentum balance (5b),

$$\nabla \cdot \langle \mathbf{u} \rangle = 0, \tag{5a}$$

$$\rho_f \frac{D\langle \mathbf{u} \rangle}{Dt} = -\nabla P + \nabla \cdot \{\mu_{\text{eff}}(\nabla \langle \mathbf{u} \rangle + {}^T\nabla \langle \mathbf{u} \rangle)\} + \mathbf{\Phi}_s(\mathbf{x},t), \tag{5b}$$

with $D\langle \mathbf{u} \rangle / Dt = \partial \langle \mathbf{u} \rangle / \partial t + \langle \mathbf{u} \rangle \cdot \nabla \langle \mathbf{u} \rangle$. The additional term $\mathbf{\Phi}_S(\mathbf{x},t)$ detailed below models the interphase coupling induced by the presence of the bubbles in the flow. The effective viscosity μ_{eff}, which differs from the molecular viscosity μ involved in the particle Reynolds number Re_p, is included in the Navier-Stokes equations (5b) to model the effects of the unresolved motions on the large-scale momentum transfer. These effects result, on the one hand, from the energy dissipation in the boundary layer and wake of each bubble, and on the other hand, from possible small-scale turbulence, i.e., from the contribution of the subgrid-scale tensor $\langle \mathbf{uu} \rangle$-$\langle \mathbf{u} \rangle \langle \mathbf{u} \rangle$. Due to the lack of specific subgrid-scale models for bubbly flows, we simply assume that μ_{eff} is constant throughout the flow.

Bubbles seeded in the flow contribute to momentum transfer and affect the bulk properties of the mixture. In Eq. (5b), $\mathbf{\Phi}_S(\mathbf{x},t)$ is an Eulerian source term distribution evolving in time and space, owing to the Lagrangian motion of the dispersed phase. Explicit formulation of this term can easily be obtained through a momentum balance over a reference volume V_f containing N_p bubbles of volume V (e.g., Refs. 35 and 36). In the limit $V_f \to 0$, this yields for particles of finite density

$$\mathbf{\Phi}_s(\mathbf{x},t) = \lim_{V_f \to 0} \frac{V}{V_f} \sum_{i=1}^{N_p} \left\{ \rho_p \left(\mathbf{g} - \frac{d\mathbf{v}^{(i)}}{dt} \right) + \rho_f \left(\frac{D\langle \mathbf{u} \rangle}{Dt} - \mathbf{g} \right) \right\}, \tag{6}$$

where the index i refers to all particles present at time t in the control volume V_f. The first term on the right-hand side of (6) is related to the reaction force acting on the ith particle and is negligibly small for bubbles. In contrast, the second term which arises from the net buoyancy force acting on the bubbles is crucial as it acts to reduce locally the net buoyancy of the large-scale flow. In classical variable-density flows, the bulk density obeys an Eulerian advection/diffusion equation. In contrast, the motion of the bubbly phase is governed by the Lagrangian equation (4). This equation clearly shows that the transport velocity of the dispersed phase may strongly differ from $\langle \mathbf{u} \rangle$ and this has deep implications on the overall dynamics of the flow.[37]

In the force balance (4), the undisturbed fluid velocity $\mathbf{u}$ has to be interpolated at the bubble location but we only solve equations for $\langle \mathbf{u} \rangle$. Therefore, we assume that unresolved small-scale fluid motions do not affect significantly the bubble trajectories and we set $\mathbf{u} = \langle \mathbf{u} \rangle$ in (4). Recent work[38] confirms that in turbulent flows computed by large eddy simulations, unresolved motions are only of minor importance for particle dispersion. Replacing $\mathbf{u}$ by $\langle \mathbf{u} \rangle$ in (4) closes the fully coupled system (4)–(6). Equations (5a) and (5b) are discretized on a staggered grid using a second-order finite volume technique. Second-order accurate time advancement is achieved by combining a third-order Runge-Kutta algorithm with a Crank-Nicolson treatment of viscous terms. Incompressibility is achieved at the end of each time step by solving a Poisson equation for a pressure correction.

We simulate a plane upflowing mixing layer seeded with bubbles rising under gravity. We assume that the most significant features of the interaction between bubbles and large-scale vortical structures are basically two dimensional. Although the computations are two dimensional, the trajectories and source term in the Navier-Stokes equations are evaluated for spherical bubbles, assuming that the void fraction is uniform in the spanwise direction. Therefore, the local void fraction is representative of the actual distribution of bubbles in a mixing layer where large-scale structures are essentially two dimensional.

The above model of two-phase bubbly flow was already successfully used in several configurations. For instance, we studied the cellular motion which can be set up when many rising bubbles are randomly injected at the bottom of a liquid layer initially at rest.[36] Detailed comparisons with experiments also proved that the model reproduces quantitatively all physical features of a bubbly plume.[37]

III. BUBBLE DISPERSION

We first consider the passive dispersion of bubbles within a plane upflowing mixing layer. The main purpose of the corresponding computations is to prepare the discussion of the two-way coupling simulations by highlighting the major role played by the large-scale coherent structures.

Numerous computational studies of the dispersion of heavy solid particles were reported in the past. The vortical structures of the flow were often computed using point vortex methods,[13,14,39] a suitable approach for situations where large-scale vortices are clearly identified. It was established that dispersion of solid particles is mainly controlled by the Stokes number, which compares the particle relaxation time to the time scale of the flow.[40] For Stokes numbers close to unity, particles are strongly swept out of vortices, a process that enhances their dispersion. This feature fully agrees with the numerical findings of Squires and Eaton,[41] who observed preferential concentration of particles in straining regions corresponding to low vorticity. Details on segregation features may be found in Ref. 1.

Considerably fewer results are available for bubbles. Lagrangian tracking of bubbles is much more time consuming because Eq. (4) requires the spatial and time derivatives of the fluid velocity to be interpolated precisely at the bubble positions, in addition to the fluid velocity itself. Ruetsch and Meiburg[42] studied bubble dispersion in a plane temporal mixing layer and showed that bubbles tend to accumulate in the vortex cores. Here we describe how bubble entrapment is related to the stable fixed points present in a plane, spatially evolving, mixing layer.

A. Location and stability of the fixed points

The presence of stable fixed points capable of producing a significant entrapment of bubbles can be proved by examining large series of trajectories or by analyzing the stability of the dynamical system governing the bubble motion. The locations of these fixed points correspond to the points of the fluid velocity field where $\mathbf{v}=\mathbf{0}$ and $d\mathbf{v}/dt=\mathbf{0}$ is a solution of the ODE (4). We may rewrite Eq. (4) in dimensionless form by introducing a velocity scale $\mathcal{U}$, a length scale L, and a time scale $T=L/\mathcal{U}$. Assuming that the flow is steady and defining the Froude number $\mathrm{Fr}=gL/\mathcal{U}^2$ and the scale ratio $\delta=2R/L$, (4) then becomes

$$\frac{1}{2}\frac{d\mathbf{v}'}{dt'}=\mathrm{Fr}\mathbf{e_x}-\frac{3}{4}\frac{C_D}{\delta}|\mathbf{v}'-\mathbf{u}'|(\mathbf{v}'-\mathbf{u}')+\frac{3}{2}\mathbf{u}'\cdot\nabla'\mathbf{u}'-\frac{1}{2}(\mathbf{v}'-\mathbf{u}')\times\boldsymbol{\omega}', \tag{7}$$

where $\mathbf{u}'=\mathbf{u}/U$, $\boldsymbol{\omega}'=\boldsymbol{\omega}L/U$, etc., and $\mathbf{e_x}$ is the unit vector along the upward vertical direction. Let $\mathbf{u}'$ have components U and V along the vertical (x) and horizontal (y) axes, respectively. Fixed points lie at the intersection of the x and y projections of (7), setting $\mathbf{v}'=\mathbf{0}$ and $d\mathbf{v}'/dt'=\mathbf{0}$. Denoting the dimensionless coordinates of the fixed point as (x_f, y_f), the system to be solved becomes

$$\begin{aligned} f_x(x_f,y_f)&=\mathrm{Fr}+\frac{1}{2}V\omega'+\frac{3}{2}(\mathbf{u}'\cdot\nabla')U+\frac{3}{4}\frac{C_D}{\delta}|\mathbf{u}'|U=0,\\ f_y(x_f,y_f)&=-\frac{1}{2}U\omega'+\frac{3}{2}(\mathbf{u}'\cdot\nabla')V+\frac{3}{4}\frac{C_D}{\delta}|\mathbf{u}'|V=0, \end{aligned} \tag{8}$$

where C_D is now the drag coefficient at the location of the fixed point, i.e., $C_D=C_D(2R\mathcal{U}|\mathbf{u}'|/\nu)$. The solution of (8) is obtained numerically. This solution yields a collection of discrete fixed points whose stability has yet to be examined to determine whether or not entrapment occurs. For this purpose we come back to Eq. (7) and first evaluate the slip velocity V_L of a single bubble rising in a quiescent liquid, which corresponds to the situation where the drag force exactly balances the buoyancy force. As experimental evidences indicate that bubbles are moving with a quasiconstant slip velocity, we may linearize the drag force about V_L. Defining the components of the actual bubble velocity as V_L+v_x and v_y, respectively, Eq. (7) may be recast in the form of a dynamical system,[10]

$$\begin{aligned} \frac{dx'}{dt'}&=v_x,\quad \frac{dy'}{dt'}=v_y,\\ \frac{dv_x}{dt'}&=2f_x(x',y')-v_y\omega'-\frac{3}{2}\frac{C_D}{\delta}V_Lv_x,\\ \frac{dv_y}{dt'}&=2f_y(x',y')+v_x\omega'-\frac{3}{2}\frac{C_D}{\delta}V_Lv_y. \end{aligned} \tag{9}$$

The Jacobian matrix of the ODE system (9) has four complex eigenvalues μ_i, which satisfy

$$\mathrm{Det}\begin{bmatrix} -\mu & 0 & 1 & 0\\ 0 & -\mu & 0 & 1\\ 2\frac{\partial f_x}{\partial x'} & 2\frac{\partial f_x}{\partial y'} & -\frac{3}{2}\frac{C_D}{\delta}V_L-\mu & -\omega'\\ 2\frac{\partial f_y}{\partial x'} & 2\frac{\partial f_y}{\partial y'} & +\omega' & -\frac{3}{2}\frac{C_D}{\delta}V_L-\mu \end{bmatrix}=0. \tag{10}$$

These eigenvalues are easily computed numerically. The last step consists in examining the sign of their real part, as it is well known that the corresponding fixed point is stable when the real part of all four eigenvalues is negative.

The above procedure was first tested on a single Lamb-Oseen vortex defined by the streamfunction

$$\psi=-C\exp\left(-\frac{r^2}{2R_c^2}\right) \tag{11}$$

with $r=(x'^2+y'^2)^{1/2}$. A bubble initially released close enough to the vortex is eventually trapped near the vortex center, whereas another one released slightly further away passes through the vortex without being trapped. Note for future purpose that the stable fixed point corresponds to a negative value of y', which according to (11) implies that the vertical velocity $U=\partial\psi/\partial y'$ is directed downwards there. A second fixed point is located outside the vortex core. This fixed point is always unstable. As long as the vortex is sufficiently strong ($V_L<U_{\max}=C/R_c^2$), the two fixed points exist and the entrapment may take place. In contrast, if $U_{\max}$ becomes smaller than V_L, no more fixed point exists because the equation $f_x(x',y'=0)$ has no more root. A detailed analysis of the forces experienced by the bubble during its spiralling trajectory reveals the major role played by the lift and added-mass forces which are both centripetal. We performed a similar study[43] for bubble entrapment in Stuart vortices[44] which are often used as an analytical model of a mixing layer. This study also showed that Stuart vortices are able to trap bubbles when the rising speed V_L of the bubbles is smaller than half the velocity difference ΔU between the two streams of the mixing layer. This defines the critical condition of entrapment based on the drift parameter $2V_L/\Delta U$.

B. Bubble dispersion in the upflowing mixing layer

We now turn to the spatially evolving upflowing mixing layer. In this case, the velocity field $\mathbf{u}$ is generated by numerical simulation of the two-dimensional Navier-Stokes equations without the coupling term $\boldsymbol{\Phi}_S$ described in Sec. II. The nonuniform grid is made of 150×50 cells. The lateral dimension of the computational domain is about six times the size of the biggest vortex while the streamwise dimension allows eight vortices to be simultaneously present in the domain. An exponential refinement of the grid is used near the inlet to capture the linear growth of the primary Kelvin-Helmholtz instability. A hyperbolic tangent velocity profile is prescribed at the inlet, while an absorbing boundary condition (see Ref. 30) is employed on the downstream boundary. The dimensionless velocity difference $\Delta U/U_m$ between the two streams is selected to be 4/3. The initial development of

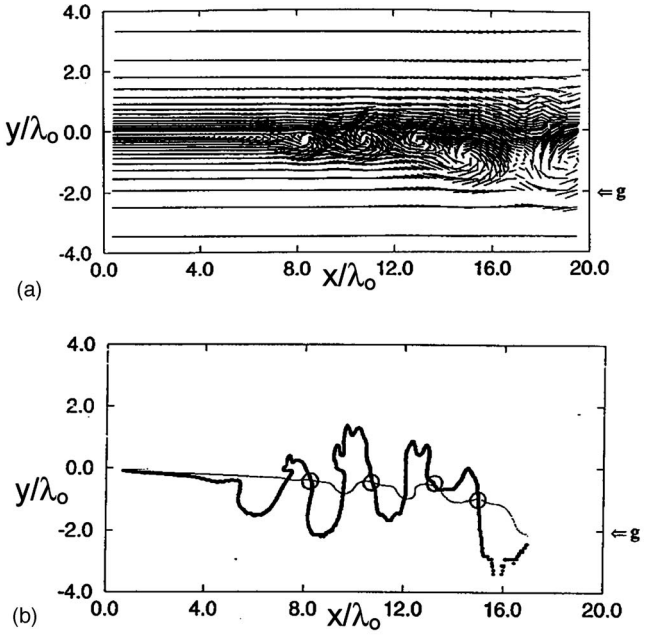

FIG. 1. Snapshot of the single-phase mixing layer. (a) Velocity field $\mathbf{u}$-$U_m\mathbf{e}_x$. (b) (○) Position of the stable fixed points ($\delta=6.94\times10^{-4}$, Fr=40). Bold line ($f_x(x,y)=0$); thin line ($f_y(x,y)=0$).

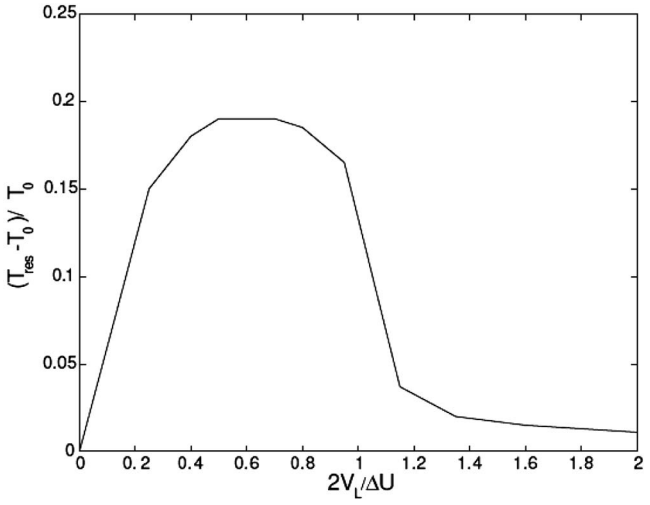

FIG. 2. Evolution of the residence time of bubbles in the mixing layer as a function of their rise velocity.

the mixing layer is triggered by numerical noise only and it was verified that the selected wavelength and frequency of the large-scale vortices are in agreement with linear theory predictions.[45] The flow Reynolds number based on the averaged fluid velocity $U_m=(U_1+U_2)/2$ and most amplified wavelength of the Kelvin-Helmholtz instability λ_o is close to 900. The latter scales are used to nondimensionalize Eqs. (8)–(10), i.e., we set $\delta=2R/\lambda_o$ and $\mathrm{Fr}=g\lambda_o/U_m^2$. Several global quantities were checked to make sure that the global behavior of the mixing layer is correct. In particular, when properly renormalized, the mean velocity profiles at different streamwise locations are found to collapse on a single hyperbolic tangent profile and the autosimilarity characteristics are achieved. The mean spreading rate was also successfully compared to the reference experimental data in Ref. 46. A snapshot of the velocity field is shown in Fig. 1(a).

To find the fixed points of the bubble trajectories and perform a stability analysis similar to that described above in an unsteady flow, a supplementary assumption is required,[47] namely that the characteristic time scale of the bubble motion is short compared to that of the flow temporal change. The Stokes number characterizing this time-scale ratio is always very small (see Table I). Making use of this assumption and substracting the average velocity $U_m\mathbf{e_x}$ from $\mathbf{u}$ (i.e., translating with the vortices), we are in position to use the methodology described in Sec. III A. The intersection of the curves $f_x=0$ and $f_y=0$ yields the fixed point locations displayed in Fig. 1(b). Each vortex clearly contains a stable fixed point [open circles in Fig. 1(b)] located near its core on the low-velocity side of the mixing layer, whereas an unstable fixed point lies in between two consecutive vortices. When the bubble radius corresponds to the critical value for which V_L equals $\Delta U/2$, the fixed points disappear, marking the end of the entrapment phenomenon. Larger bubbles with $V_L>\Delta U/2$ pass through the vortices without being trapped.

We examine bubble dispersion by injecting bubbles close to the inflexion point of the inlet velocity profile. Bubbles are released with their terminal slip velocity V_L. The role of the coherent vortices can easily be appreciated by comparing the mean time required for bubbles of different sizes, i.e., different V_L, to reach the upper bound of the domain. In the absence of coherent vortices, the residence time T_{res} of a bubble of terminal velocity V_L would simply be $T_0=H/(U_m+V_L)$, with H being the height of the domain. The relative variation of T_{res} is plotted versus the entrapment parameter $2V_L/\Delta U$ in Fig. 2. As expected from the above discussion, large bubbles (corresponding to $2V_L/\Delta U>1$) merely pass through the vortices without being trapped, so that T_{res} is only weakly affected by the presence of the vor-

TABLE I. The nondimensional numbers characterizing the two-way coupling simulations.

	Local void fraction	Scale ratio 2R/L	Drift parameter $V_L/\mathcal{U}$	Stokes number $\tau_p/(L/\mathcal{U})$	Reynolds number Re_p
Isolated vortex	1%	3.10^{-3}	0.6	2.65×10^{-3}	310
Mixing layer					
Case B	0.25%	6.94×10^{-4}	0.75	9.72×10^{-4}	310
Case C	0.5%	6.94×10^{-4}	0.75	9.72×10^{-4}	310
Case D	0.5%	9.02×10^{-4}	1.25	1.52×10^{-3}	650

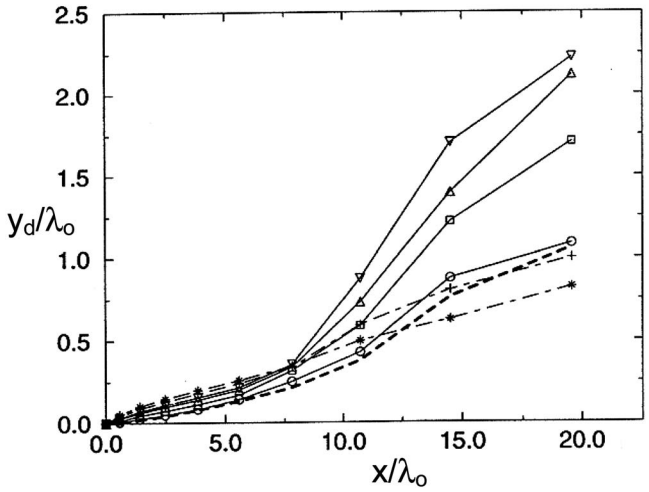

FIG. 3. Lateral dispersion of bubbles of various sizes in the mixing layer. (Dashed line) Fluid particle; (○) $\delta=2.77\times10^{-4}$; (□) $\delta=5.55\times10^{-4}$; (△) $\delta=6.94\times10^{-4}$; (▽) $\delta=7.63\times10^{-4}$; (+) $\delta=9.02\times10^{-4}$; (*) $\delta=10.4\times10^{-4}$.

tices. In contrast, the residence time of smaller bubbles may increase by about 20%, especially in the range $0.4<2V_L/\Delta U<0.9$. For such bubbles the average rise velocity is not U_m+V_L anymore, but rather U_m, as they are essentially translating with the vortices. Trajectories of bubbles corresponding to values of V_L much smaller than $\Delta U/2$ are close to paths of fluid elements, so that T_{res} tends towards T_0 as V_L tends to zero. Similar features were noticed in experiments performed by Poorte and Biesheuvel[48] in homogeneous isotropic turbulence. More precisely, their measurements revealed that the residence time of millimetric bubbles in a vertical water tunnel increased by about 30% when the flow was turbulent, as compared to the residence time determined in quiescent water.

It is customary to describe particle dispersion by evaluating the streamwise variation of the lateral dispersion function. For this purpose the whole domain is sliced into ten subdomains of height $H/10$. The standard deviation y_d of the lateral displacement is evaluated in each subdomain by averaging on all positions of bubbles located within this slice. Figure 3 displays the variation of $y_d(x)$ versus the bubble diameter. Close to the inlet ($x/\lambda_o<7$), the lateral dispersion is weak because no rollup takes place in this early region. Bubble trajectories are thus close to paths of fluid elements. As coherent structures develop further downstream, the lateral dispersion increases and two distinct behaviors are observed. Bubbles corresponding to $\delta>9.0\times10^{-4}$ ($2V_L/\Delta U=1.25$) pass through the vortices and eventually disperse less than fluid elements. In contrast, smaller bubbles are trapped by the vortices and follow trajectories close to a cycloid. The lateral dispersion of such bubbles increases with their diameter. The reason for this may be understood by examining how the average lateral position of the fixed points change with δ. Increasing δ tends to tilt this mean lateral position toward the low-velocity side, forcing the bubbles to experience lateral displacements larger than those of the vortex centers. A similar trend was observed in Ref. 42 in the case of a single vortex.

IV. TWO-WAY COUPLING EFFECTS

As small enough bubbles are attracted toward the core of coherent vortices, the local volume fraction of the dispersed phase tends to increase. These are the regions where the dynamics of the mixing layer are expected to be primarily affected by interphase coupling mechanisms. To gain some insight into the consequences of these mechanisms, we perform two-way coupling computations based on the model discussed in Sec. II. We assume that the effective viscosity of the bubbly flow is constant and that the spatially evolving mixing layer may be considered as a two-dimensional transitional flow. Again, before we examine the modifications of the spatially evolving mixing layer, we briefly discuss the evolution of a single vortex seeded with small bubbles, as it represents a canonical situation where the successive stages of the interaction process may easily be disentangled.

A. Evolution of a single vortex

To this end, we solve the coupled equations (4)–(6) in the case of the Lamb-Oseen vortex [Fig. 4(a)] already considered in Sec. III. Two-way coupling interactions are enforced by injecting bubbles close to the stable fixed point of the vortex. Once trapped, the bubbles spiral around the fixed point and transfer momentum to the fluid. As buoyancy provides the dominant contribution in the coupling source term [Eq. (6)], the transferred momentum is essentially directed vertically upward. Consequently, the local vertical velocity experiences a positive disturbance [Fig. 4(b)]. Since the vertical velocity of the undisturbed vortex (say U_0) is negative in the vicinity of the fixed point (see Sec. III A), the magnitude of the disturbed vertical velocity U is smaller than $|U_0|$. As the vertical velocity remains almost zero at $x'=y'=0$, the magnitude of the transverse gradient of the vertical velocity $\partial U/\partial y'$ is reduced compared to that of $\partial U_0/\partial y'$ (Fig. 5). A similar behavior was observed in point-force computations of bubbly homogeneous isotropic turbulence.[18] From Eq. (7), it is clear that the reduction of $\partial U/\partial y'$ lowers the radial component of the added-mass force, i.e., the strength of the dominant centripetal force. As the capture process proceeds, the cumulative strength of the above effect increases, making the stable fixed point move away from the vortex center to stay in a region of the flow where the negative vertical velocity remains comparable to U_0 [Figs. 6(a)–6(c)]. When the number of bubbles captured within the vortex exceeds a critical value, there is no more point within the vortex at which the combined requirement of a strong centripetal force and a sufficiently negative vertical velocity can be simultaneously satisfied, so that the fixed point becomes unstable. Bubbles are then released out of the vortex, which recovers its initial characteristics [Fig. 6(d)]. In particular, the fixed point becomes stable again, enabling entrapment and initiating a new interaction cycle. Thus, provided bubbles are continuously injected, periodic cycles during which the fixed points are successively stable and unstable take place. Similar features were observed numerically in Ref. 21 and experimentally in Ref. 4. Indeed, the latter experiments proved that even few microscopic bubbles are able to modify dramatically the position of a vortex and the velocity gradients within it. More

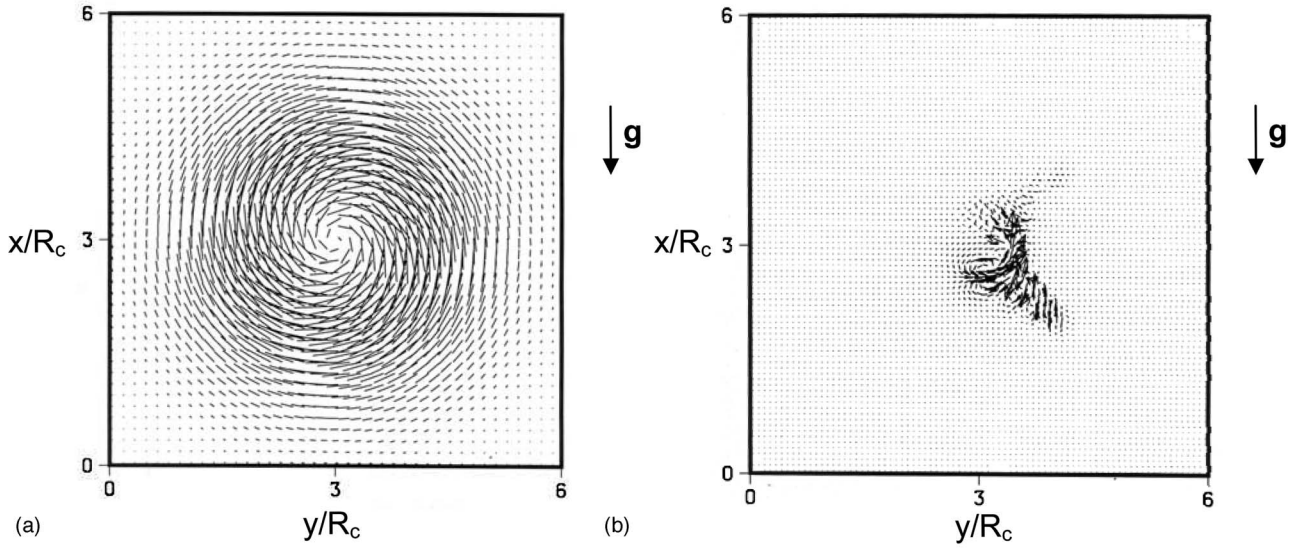

FIG. 4. Effect of a single bubble on the velocity field of a Lamb-Oseen vortex. (a) Single-phase flow; (b) disturbance induced by a trapped bubble.

precisely, the injection of five 512 μm diameter bubbles in the vortex was observed to displace the vortex core by 3.5 mm upward. The buoyancy forcing term induces modifications of the local velocity gradients and vorticity peaks which are found to increase by about 20% compared to their original value. In our simulations, the maximum local void fraction is less than 1% when the stable fixed point loses its stability. Velocity perturbations are in the range of 2% of the maximum velocity $U_{\max}$, and the local vorticity variation due to two-way coupling is around 20% of the local undisturbed vorticity level. However the most noticeable effect of interphase coupling is the release of bubbles initially trapped within the vortex core. Passive bubbles would have stayed entrained by the vortex core for much longer times. Obviously, none of the above phenomena takes place if the injected bubbles pass through the vortex without being trapped (drift parameter $V_L/U_{\max} > 1$). Then the interaction time is very short and only weak modifications of the flow are observed.

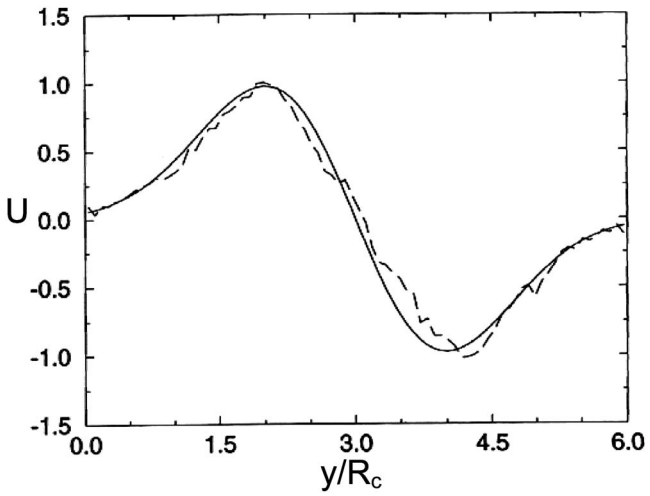

FIG. 5. Bubble-induced modification in the vertical velocity profile. (Solid line) Single-phase flow; (dashed line) two-phase flow.

B. Spatially evolving mixing layer

In Sec. III we showed that small enough bubbles ($V_L < \Delta U/2$) accumulate in the large-scale vortical structures of the mixing layer. Therefore, owing to the local increase of the volume fraction, we expect two-way coupling effects to produce local modifications of the flow similar to those discussed above. These modifications may in turn influence the global features of the flow field. To explore such phenomena, two-way coupling computations are carried out in three different situations (cases B, C, and D). The reference case (case A) is the single-phase flow described in Sec. III where bubbles are tracked in the flow but Φ_S is set to zero. Case B corresponds to a 0.25% average volume fraction of bubbles

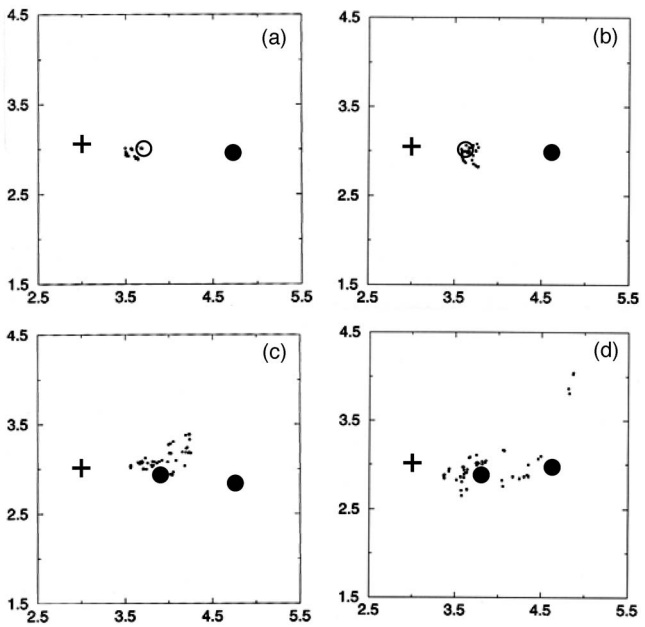

FIG. 6. Evolution of the bubble positions (small dots) within the vortex as a function of the number of bubbles (a–d). Location of the: (+) vortex center, (○) stable fixed point, and (●) unstable fixed point. The simulation domain is similar to that in Fig. 4.

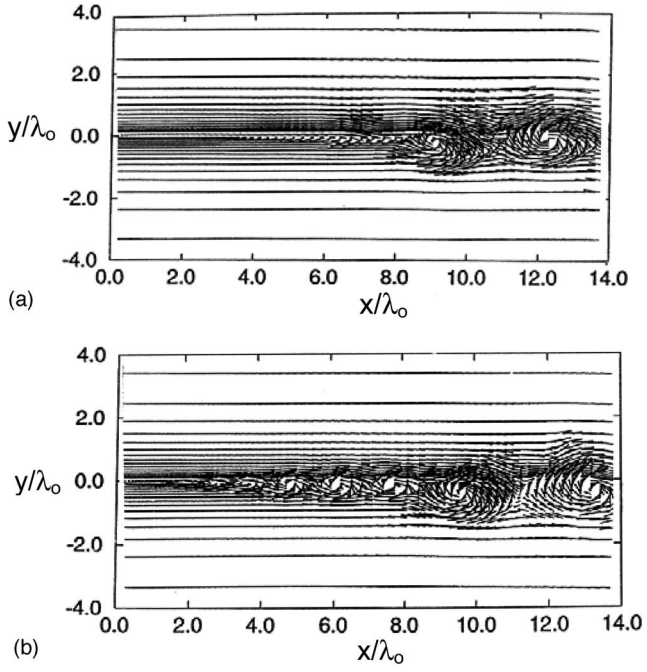

FIG. 7. Snapshot of the velocity field of the carrying flow close to the inlet section. (a) Single-phase flow (case A); (b) two-phase flow (case B).

with $\delta=6.94\times10^{-4}$. These bubbles are expected to be trapped by the vortices since they satisfy the criterion $V_L < \Delta U/2$. Case C is identical to case B, except that the average volume fraction is increased to 0.50%. Finally, case D has the same average volume fraction as case B, but with larger bubbles corresponding to $\delta=9.02\times10^{-4}$. According to the results of Sec. III, these bubbles are not captured by the vortices. All bubbles are injected around the inflection point of the velocity profile in the inlet section. The simulation conditions are referenced in Table I. The parameters we selected correspond to bubbles of 1 mm and 1.3 mm diameter rising in water. The extremely low value of the Stokes number clearly indicates that the bubbles respond very quickly to fluid flow fluctuations. The typical length scale L is the wavelength of the mixing layer λ_o and the drift parameter is based on $\Delta U/2$. The assumption that bubbles are small compared to the vortical structures agrees with the experimental conditions of Roig *et al.*[20] In these experiments, the typical size of the vortices is 10 cm at 40 cm from the inlet section and the bubble diameter is about 2 mm.

Near the inlet section, i.e., in the region where the disturbances grow linearly due to the Kelvin-Helmholtz instability, all two-phase flows display the same behavior. The comparison of Figs. 7(a) and 7(b) indicates that the first pairing occurs much earlier in the two-phase case, which suggests that the small-scale disturbances produced by the bubbles trigger efficiently the rollup phenomenon. Local void fraction fluctuations act as a random forcing of the mixing layer. The typical length scale of these perturbations is ten times larger than the bubble diameter while the spatial resolution scale λ of our simulations is intermediate between the bubble diameter and the large-scale features of the two-dimensional mixing layer. A spectral analysis of the flow field confirms the visual observation that the selected wavelength of the coherent vortices is the same as in the single-phase situation, i.e., λ_0. This result is in agreement with that obtained for solid particles through a linear stability analysis.[49]

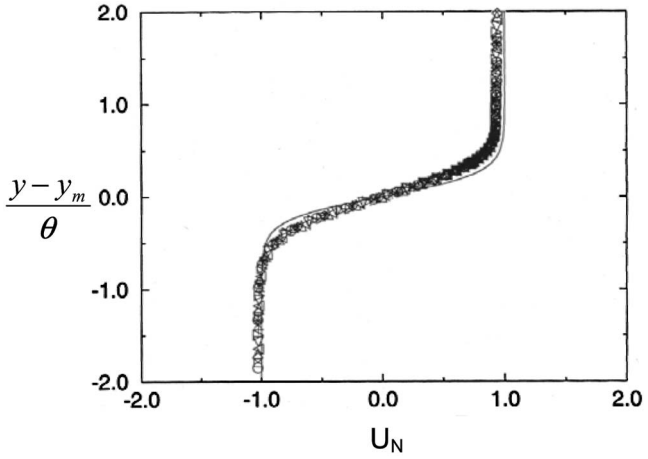

FIG. 8. Profiles of the normalized streamwise velocity $U_N=(U(x,y)-U_m(x))/\Delta U(x)$ vs the dimensionless lateral position $(y-y_m(x))/\theta(x)$. Symbols correspond to distinct streamwise locations. (Solid line) tanh profile.

In order to study the effects of the dispersed phase on the global flow characteristics, it is of high interest to average the fluid velocity in time. Let $\bar{U}(x,y)$ be the corresponding time-averaged streamwise velocity. Figure 8 shows several profiles of the normalized velocity $U_N(\eta)=2(\bar{U}(x,y)-U_m(x))/\Delta U(x)$ plotted versus the dimensionless lateral position $\eta=(y-y_m(x))/\theta(x)$. Here $y_m(x)$ is the position of the flow centerline (i.e., $\bar{U}(x,y_m(x))=U_m(x)$) and $\theta(x)$ is the local thickness of the mixing layer defined as the lateral distance between the two points where $U_N=\pm0.475$. All profiles corresponding to cases B through D collapse on a master curve, whatever the streamwise location (see Ref. 8 for a similar trend on bubble concentration). This result indicates that the streamwise velocity achieves self-similarity in such low-concentration bubbly mixing layers. A similar conclusion was reached experimentally in Ref. 20. Figure 9 shows the streamwise evolution of the centerline position for the single

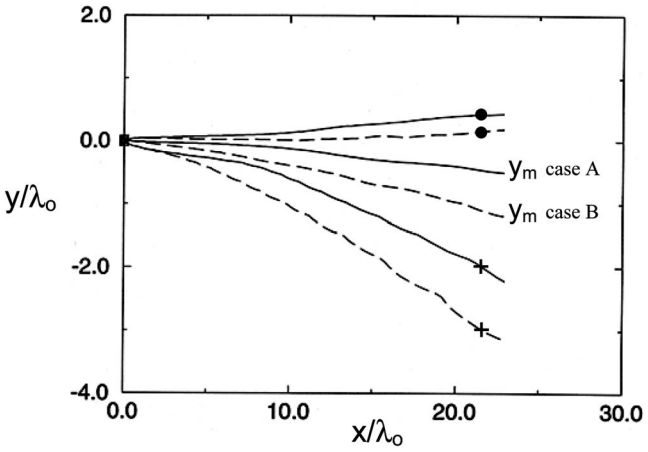

FIG. 9. Streamwise evolution of the average centerline position $y_m(x)$. (Solid line) Case A; (dashed line) case B; (●) $y(0.9U_2)$; (+) $y(1.1U_1)$.

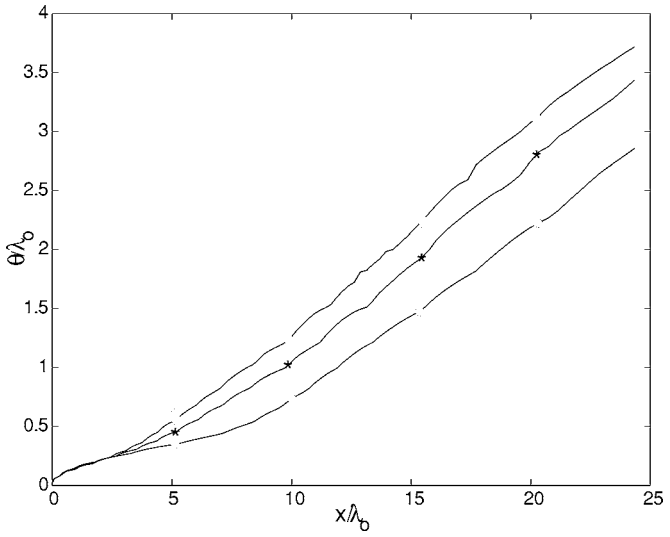

FIG. 10. Streamwise evolution of the mixing layer thickness $\theta(x)$. (○) Case A; (∗) case B; (◇) case C.

phase (case A) and the bubbly mixing layer (case B). Compared to the single-phase situation, the bubbly mixing layer appears to be strongly tilted toward the low-velocity side.[8] Single-phase spatially developing mixing layers are known to be already tilted toward this side (see the curve corresponding to case A in Fig. 9) because the entrainment rate of the high-speed fluid is larger than that of the low-speed stream.[50] In a bubbly flow where bubble entrapment takes place, this feature is reinforced by the two-way coupling mechanism which induces a baroclinic effect for the following reason. Bubbles rising in the central part of the flow spend part of their time spiraling around the fixed points of the vortices as we saw in Sec. IV A. Therefore, the time-averaged density of the two-phase medium has a minimum at the average lateral position of the stable fixed points, which we know to be located on the low-velocity side of the mixing layer (see Sec. III B). "Heavy" fluid thus tends to invade this relatively light region. For the same reason as in a single-phase flow, most of this heavy fluid comes from the high-velocity side. Therefore, there is a net increase of the local streamwise velocity which results in a bending of the average centerline towards the low-velocity side. Figure 10 displays the streamwise evolution of the mixing layer thickness. As may be expected on the grounds of Fig. 7, the linear growth of θ starts much closer to the inlet section in the two-phase cases. Moreover, beyond $x/\lambda_0 \approx 3$, the slope $d\theta/dx$ is found to be strongly increased in the presence of small bubbles (cases B and C). This effect obviously increases with the volume fraction of bubbles. For instance, near the downstream boundary of the domain ($x/\lambda_0 \approx 25$), $\theta(x)$ is about 20% larger in case B than in the single-phase situation, whereas the increase reaches 30% in case C, where the average bubble concentration is twice that of case B. The main mechanism responsible for this fairly spectacular increase of $d\theta/dx$ appears to be the meandering of the large-scale vortices. Indeed, for the reason discussed above, during the stage corresponding to the bubble capture, a coherent vortex tends to move towards the low-velocity side. In contrast, the local density of the two-phase mixture is made more homogeneous after the bubbles have been released for this vortex, so that it tends to move back toward the high-velocity side during this second stage. In a time-averaged view, this alternate motion results in an increased lateral mixing, i.e., in an increase of $d\theta/dx$. Qualitatively similar trends for both the lateral tilting and the spreading rate were observed in Ref. 20, where millimetric bubbles (with an average diameter about 2 mm) were injected with a volume fraction up to 3% at the bottom of an upward mixing layer. Similar conclusions for the spatial growth of the vorticity thickness were also obtained numerically in Ref. 24 using an Eulerian-Lagrangian approach.

In the presence of bubbles such as $2V_L/\Delta U > 1$ (case D), the global parameters of the mixing layer differ by less than 5% from those of the single-phase flow. It was already reported in Ref. 19 (where the experiments were carried out with bubbles with a typical diameter of about 4 mm) that a dispersed phase made of "large" bubbles only marginally affect the global dynamics of upward mixing layers. The reason for the dramatic difference observed between cases B/C and case D (or between the experimental results of Refs. 19 and 20) in the streamwise evolution of the global flow parameters is clearly related to the entrapment phenomenon and its consequences on the life cycle of the large-scale vortices. Present results establish that for a given bubble volume fraction, the large-scale features of the time-averaged flow may or may not be deeply modified by the presence of bubbles, depending on whether or not they satisfy the entrapment criterion. If they do, they alter the dynamics of the coherent vortices as described in Sec. IV A and their preferential concentration within these vortices during part of their residence time produces a baroclinic effect that affects the position of the centerline and the thickness of the mixing layer. If they do not, their interaction time with a given vortex is short. Moreover, their spatial distribution within the flow is fairly homogeneous, and so is the distribution of the momentum they transfer to the fluid. These two features make bubbles produce only minor changes in the large-scale flow when $V_L > \Delta U/2$.

The last result provided by these computations concerns the lateral dispersion of bubbles in cases B and C, where the dynamics were found to be deeply modified by the interphase transfer. Figure 11 shows that two-way coupling effects strongly reduce this lateral dispersion. This is essentially because the fixed point of each vortex, which is stable in the single-phase configuration (case A), is unstable during part of the residence time of the bubbles in cases B and C, owing to the reduction of the added-mass force described in Sec. IV A. During the stage where a given vortex has no stable fixed point, the bubbles released out of this vortex accumulate on the high-velocity side of the mixing layer, instead of staying on the low-velocity side in case A [see Figs. 12(a) and 12(b)]. The time-averaged consequence of this difference is a decrease of the lateral dispersion function compared to that found in case A. Obviously, the lateral dispersion function of bubbles with $V_L > \Delta U/2$ experiences little modifications compared to the single-phase situation.

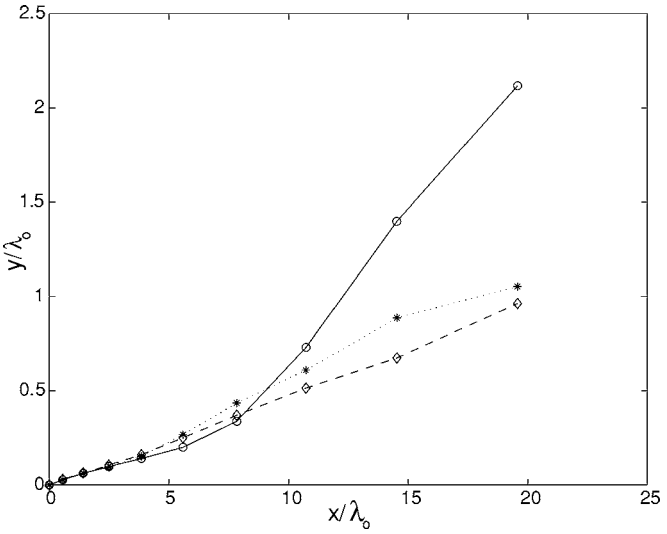

FIG. 11. Streamwise evolution of the lateral dispersion. (○) Case A; (∗) case B; (◇) case C.

V. SUMMARY AND CONCLUSIONS

In this paper we used a computational approach to investigate various aspects of the dynamics of a plane upflowing mixing layer in presence of a dispersed phase made of spherical isolated bubbles. We employed a Lagrangian description of the dispersed phase in which the total hydrodynamic force acting on each bubble comprises buoyancy, a viscous drag, a pressure gradient contribution, an added-mass force, and a shear-induced lift force. We first carried out one-way coupling simulations to determine how bubbles of different diameters disperse in the coherent vortices of the mixing layer. For this purpose, we performed a stability analysis of the fixed points present in these vortices to find out the critical conditions for preferential accumulation of bubbles. We showed that small enough bubbles are trapped within these vortices, owing to the centripetal action of inertial forces. In contrast, bubbles whose velocity (i.e., diameter) exceeds a critical value cannot be trapped and escape from the vortices. The residence time of the former category of bubbles was found to be roughly 20% larger than that of the second category. Similarly, the lateral dispersion of bubbles trapped in the vortices was found to be significantly larger than (frequently twice as large as) that of bubbles whose rise velocity exceeds the critical condition $V_L = \Delta U/2$. This is because the former bubbles follow cycloidal trajectories with lateral displacements increasing with the drift parameter $2V_L/\Delta U$, whereas the larger ones merely cross the vortices and disperse even less than fluid elements.

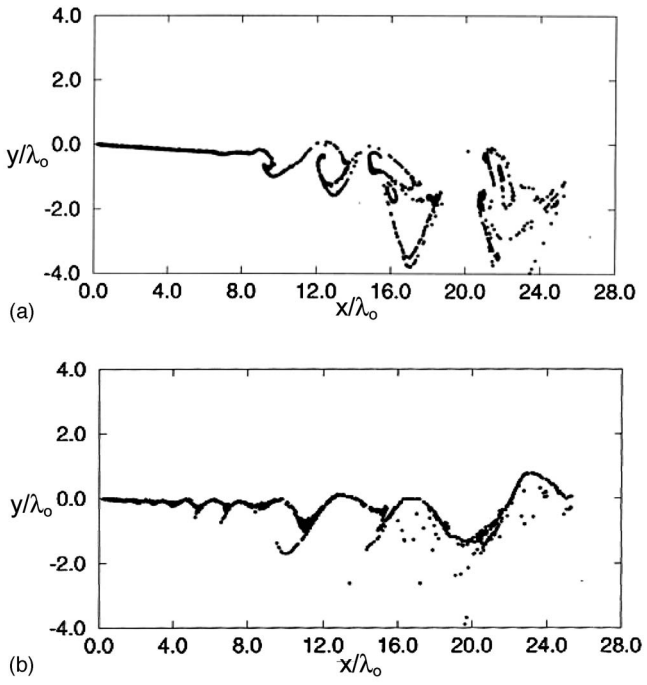

FIG. 12. Instantaneous positions of bubbles in the mixing layer. (a) Case A; (b) case B.

We studied the effect of the dispersed phase on the motion of the carrying flow using a two-way coupling approach based on a point-force approximation. In this approach, the interphase momentum transfer term which results from the presence of the bubbles tends to reduce the net acceleration of the surrounding fluid, essentially through a buoyancy effect. Using this formulation, we first examined the evolution of a single Lamb-Oseen vortex forced by some bubbles satisfying the entrapment criterion. The buoyancy transferred to the fluid was found to decrease the magnitude of the (negative) vertical velocity in the vicinity of the stable fixed point, resulting in a significant reduction of the transverse gradient of this vertical velocity. This effect reduces the centripetal forces acting on the bubbles and the fixed point eventually becomes unstable. The bubbles are then released out of the vortex, allowing a new cycle of interaction to take place. Ruetsch and Meiburg[42] found that there is an intermediate bubble size for which the coupling effect is maximum. This optimum is related to the existence of equilibrium points for both the bubble trajectories and the local concentration of bubbles. They noticed that two-way coupling effects modify the location and the level of the local accumulation of bubbles. Our simulations display the same features. This preliminary study was found useful to interpret the evolution of the upflowing mixing layer forced by bubbles. Indeed the same sequence takes place with small enough bubbles, yielding important modifications of the global characteristics of the time-averaged flow field. In particular, we noticed that the centerline of the corresponding two-phase mixing layers is tilted towards the low-velocity side, while their thickness increases much more rapidly than in the single-phase case. We interpreted the former feature as being due to the baroclinic effect resulting from the part-time entrapment of the bubbles in the coherent vortices, the consequence of which is to create a region of lighter two-phase mixture on the low-velocity side. We pointed out that the alternance of such periods during which the mixture density is inhomogeneous within a given vortex, and of periods during which this density is homogeneous because bubbles are released toward the high-velocity side, results in a lateral meandering of the large-scale vortices. This meandering phenomenon is responsible for the observed increase of the spreading rate of the time-averaged mixing layer. We also noticed that the lateral

dispersion of these bubbles is reduced compared to the one-way situation, due to periods of time during which the fixed point of each vortex is unstable. In contrast with these results, the effects of larger bubbles ($2V_L/\Delta U > 1$) on the flow field were found to be weak because such bubbles merely rise through the vortices and have only a short interaction time with each of them. These two contrasted behaviors are in line with available experimental results[19] (4 mm bubble diameter) and Ref. 20 (2 mm bubble diameter). Hence it turns out that, despite the simplifying assumptions we used (especially that of a two-dimensional flow field), the present two-way coupling investigation of a low-concentration bubbly flow, combined with a dynamical system approach of bubble motion within the coherent vortices, was able to reconcile these apparently conflicting experimental conclusions and to provide physical explanations for the observed behaviors.

[1] J. K. Eaton and J. R. Fessler, "Preferential concentration of particles by turbulence," Int. J. Multiphase Flow **20**, 169 (1994).
[2] P. D. M. Spelt and A. Biesheuvel, "On the motion of gas bubbles in homogeneous isotropic turbulence," J. Fluid Mech. **336**, 221 (1997).
[3] J. Davila and J. C. R. Hunt, "Settling of small particles near vortices and in turbulence," J. Fluid Mech. **440**, 117 (2001).
[4] G. Sridhar and J. Katz, "Effect of entrained bubbles on the structure of vortex rings," J. Fluid Mech. **397**, 171 (2001).
[5] P. M. Rightley and J. C. Lasheras, "Bubble dispersion and interphase coupling in a free-shear flow," J. Fluid Mech. **421**, 21 (2000).
[6] B. Ford and E. Loth, "Forces on ellipsoidal bubbles in a turbulent shear layer," Phys. Fluids **10**, 178 (1998).
[7] T. Dreier, S. Blaser, W. Kinzelbach, M. Virant, and H. G. Maas, "Simultaneous measurement of particle and fluid velocities in a plane mixing layer with dispersion," Exp. Fluids **29**, 486 (2000).
[8] C. Martinez-Bazan and J. C. Lasheras, "Turbulent dispersion of bubbles in a plane free shear layer," Exp. Therm. Fluid Sci. **25**, 437 (2001).
[9] J. C. R. Hunt, T. R. Auton, K. Sene, N. H. Thomas, and R. Kowe, "Bubble motions in large eddies and turbulent flows," in *Transient Phenomena in Multiphase Flow*, edited by N. H. Afghan (Hemisphere, Washington, DC, 1988), pp. 103–126.
[10] K. K. Tio, A. Liñan, J. C. Lasheras, and A. M. Gañan-Calvo, "On the dynamics of buoyant and heavy particules in a periodic Stuart vortex flow," J. Fluid Mech. **254**, 671 (1993).
[11] K. K. Tio, J. C. Lasheras, A. M. Gañan-Calvo, and A. Liñan, "The dynamics of bubbles in periodic vortex flows," Appl. Sci. Res. **51**, 285 (1993).
[12] M. R. Maxey, "The motion of small spherical particles in a cellular flow field," Phys. Fluids **30**, 1915 (1987).
[13] R. Chein and J. N. Chung, "Effects of vortex pairing on particle dispersion in turbulent shear flows," Int. J. Multiphase Flow **13**, 785 (1987).
[14] R. Chein and J. N. Chung, "Simulation of particle dispersion in a two-dimensional mixing layer," AIChE J. **34**, 946 (1988).
[15] K. D. Squires and J. K. Eaton, "Particle response and turbulence modification in isotropic turbulence," Phys. Fluids A **2**, 1191 (1990).
[16] S. Elghobashi and G. C. Truesdell, "On the two-way interaction between homogeneous turbulence and dispersed solid particles. Part I: Turbulence modification," Phys. Fluids A **5**, 1790 (1993).
[17] Q. Wang and K. D. Squires, "Large eddy simulation of particle-laden turbulent channel flow," Phys. Fluids **8**, 1207 (1996).
[18] I. M. Mazzitelli, D. Lohse, and F. Toschi, "On the relevance of the lift force in bubbly turbulence," J. Fluid Mech. **488**, 283 (2003).
[19] E. Loth and M. S. Cebrinzky, "Modulation of shear layer thickness due to large bubbles," Int. J. Multiphase Flow **21**, 919 (1995).
[20] V. Roig, C. Suzanne, and L. Masbernat, "Experimental investigation of a bubbly mixing layer," Int. J. Multiphase Flow **24**, 35 (1998).
[21] G. R. Ruetsch and E. Meiburg, "Two-way coupling in shear layer with dilute bubble concentrations," Phys. Fluids **6**, 2656 (1994).
[22] E. Meiburg, E. Wallner, A. Pagella, A. Riaz, E. Hartel, and F. Necker, "Vorticity dynamics of dilute two-way coupled particle-laden mixing layers," J. Fluid Mech. **421**, 185 (2000).
[23] E. Wallner and E. Meiburg, "Vortex pairing in two-way coupled, particle laden mixing layers," Int. J. Multiphase Flow **28**, 325 (2002).
[24] O. A. Druzhinin and S. E. Elgobashi, "Direct numerical simulation of a three-dimensional spatially developing bubble-laden mixing layer with two-way coupling," J. Fluid Mech. **429**, 23 (2001).
[25] R. Gatignol, "The Faxen formulae for a rigid particle in unsteady non-uniform Stokes flow," J. Mec. Theor. Appl. **1**, 143 (1983).
[26] M. R. Maxey and J. J. Riley, "Equation of motion for a small rigid sphere in a non-uniform flow," Phys. Fluids **26**, 883 (1983).
[27] G. Mougin and J. Magnaudet, "Path instability of a rising bubble," Phys. Rev. Lett. **88**, 014502 (2002).
[28] J. Magnaudet and I. Eames, "The motion of high-Reynolds-number bubbles in inhomogeneous flows," Annu. Rev. Fluid Mech. **32**, 659 (2000).
[29] J. Magnaudet, "Inertial effects of a spherical bubble, drop or particle moving near a wall in a time-dependent linear flow," J. Fluid Mech. **485**, 115 (2003).
[30] J. Magnaudet, M. Rivero, and J. Fabre, "Accelerated flows past a rigid sphere or a spherical bubble. Part I: Steady straining flow," J. Fluid Mech. **284**, 97 (1995).
[31] D. W. Moore, "The boundary layer on a spherical gas bubble," J. Fluid Mech. **16**, 161 (1963).
[32] M. Rivero, J. Magnaudet, and J. Fabre, "Quelques résultats nouveaux concernant les forces exercées sur une inclusion sphérique par un écoulement accéléré," C. R. Acad. Sci., Ser. II: Mec., Phys., Chim., Sci. Terre Univers **312**, 1499 (1991).
[33] D. Legendre and J. Magnaudet, "The lift force on a spherical bubble in a viscous linear shear flow," J. Fluid Mech. **368**, 81 (1998).
[34] T. R. Auton, "The lift force on a spherical body in a rotational flow," J. Fluid Mech. **183**, 199 (1987).
[35] E. Climent and J. Magnaudet, "Simulation d'écoulements induits par des bulles dans un liquide initialement au repos," C. R. Acad. Sci., Ser. IIb: Mec., Phys., Chim., Astron. **324**, 91 (1997).
[36] E. Climent and J. Magnaudet, "Large-scale simulations of bubble-induced convection in a liquid layer," Phys. Rev. Lett. **82**, 4827 (1999).
[37] O. Caballina, E. Climent, and J. Dusek, "Two-way coupling simulations of instabilities in a plane bubble plume," Phys. Fluids **15**, 1535 (2003).
[38] V. Armenio, U. Piomelli, and V. Fiorotto, "Effect of the subgrid scales on particle motion," Phys. Fluids **11**, 3030 (1999).
[39] F. Wen, N. Kamalu, J. N. Chung, C. T. Crowe, and T. R. Troutt, "Particle dispersion by vortex structures in plane mixing layers," J. Fluids Eng. **114**, 657 (1992).
[40] K. Hishida, A. Ando, and M. Maeda, "Experiments on particle dispersion in a turbulent mixing layer," Int. J. Multiphase Flow **18**, 181 (1992).
[41] K. D. Squires and J. K. Eaton, "Preferential concentration of particules by turbulence," Phys. Fluids A **3**, 1169 (1991).
[42] G. R. Ruetsch and E. Meiburg, "On the motions of small spherical bubbles in two-dimensional vortical flows," Phys. Fluids A **5**, 2326 (1993).
[43] E. Climent and J. Magnaudet, "Modifications d'une couche de mélange verticale en présence de bulles," C. R. Acad. Sci., Ser. IIb Mec. Phys. Astron. **326**, 627 (1998).
[44] J. T. Stuart, "On finite amplitude oscillations in laminar mixing layers," J. Fluid Mech. **29**, 417 (1967).
[45] P. A. Monkewitz and P. Huerre, "Absolute and convective instabilities in free shear layers," J. Fluid Mech. **159**, 151 (1985).
[46] D. Oster and I. Wygnanski, "The forced mixing layer between parallel streams," J. Fluid Mech. **123**, 91 (1982).
[47] C. W. Stewart and C. T. Crowe, "Bubble dispersion in free shear flows," Int. J. Multiphase Flow **19**, 501 (1993).
[48] R. E. G. Poorte and A. Biesheuvel, "Experiments on the motion of gas bubbles in turbulence generated by an active grid," J. Fluid Mech. **461**, 127 (2002).
[49] Y. Yang, J. N. Chung, T. R. Troutt, and C. T. Crowe, "The influence of particles on the spatial stability of two-phase mixing layers," Phys. Fluids A **2**, 1839 (1990).
[50] P. S. Lowery and W. C. Reynolds, "Numerical simulation of a spatially developing, forced, plane mixing layer," Department of Mechanical Engineering, Stanford University, CA Report No. TF-26, 1986.